

**Structure of eutectic liquids in the Au-Si, Au-Ge, and Ag-Ge binary systems by neutron diffraction**Prae Chirawatkul,<sup>1</sup> Anita Zeidler,<sup>1</sup> Philip S. Salmon,<sup>1</sup> Shin'ichi Takeda,<sup>2</sup> Yukinobu Kawakita,<sup>3</sup> Takeshi Usuki,<sup>1,\*</sup> and Henry E. Fischer<sup>4</sup><sup>1</sup>*Department of Physics, University of Bath, Bath BA2 7AY, United Kingdom*<sup>2</sup>*Department of Physics, Faculty of Sciences, Kyushu University, 6-10-1 Hakozaki, Higashi-ku, Fukuoka 812-8581, Japan*<sup>3</sup>*Neutron Science Section, Materials and Life Science Facility Division, J-PARC Center, Japan Atomic Energy Agency, 2-4 Shirakata Shirane, Tokai, Naka, Ibaraki 319-1195, Japan*<sup>4</sup>*Institut Laue-Langevin, 6 rue Jules Horowitz, Boîte Postale 156, F-38042, Grenoble Cédex 9, France*

(Received 12 October 2010; published 18 January 2011)

Neutron diffraction was used to investigate the structure of the liquid alloys  $\text{Au}_{0.81}\text{Si}_{0.19}$ ,  $\text{Au}_{0.72}\text{Ge}_{0.28}$ , and  $\text{Ag}_{0.74}\text{Ge}_{0.26}$  with composition at or near the eutectic. For a given alloy, the measured pair distribution function is described over a wide range of distances, from 5–6 Å to beyond 20 Å, by an exponentially damped oscillatory function with a decay length and wavelength of oscillation related to the half-width at half-maximum of the principal peak in the total structure factor and to the position of this peak, respectively. This behavior is expected from solutions of the Ornstein-Zernike equations for simple pair potentials. There is no need to invoke the existence of a fractal network, as suggested by a recent analysis of the diffraction patterns measured for amorphous metallic alloys, to account for the experimental results. A reconsideration of the diffraction data for these amorphous alloys points to the same conclusion.

DOI: [10.1103/PhysRevB.83.014203](https://doi.org/10.1103/PhysRevB.83.014203)

PACS number(s): 61.25.Mv, 61.05.fm, 61.05.cp

**I. INTRODUCTION**

The phase diagrams of the binary Au-Si, Au-Ge, and Ag-Ge systems do not show the formation of stable compounds, but each has a deep eutectic region where the melting point decreases to 363 °C for  $\text{Au}_{0.814}\text{Si}_{0.186}$  (Ref. 1), 361 °C for  $\text{Au}_{0.72}\text{Ge}_{0.28}$  (Ref. 2), and 651 °C for  $\text{Ag}_{0.755}\text{Ge}_{0.245}$  (Ref. 3) as compared with melting points of 962, 1064, 1414, and 938 °C for pure Ag, Au, Si, and Ge, respectively. A deep eutectic is often an indicator of good glass-forming ability, and Au-Si was the first metallic alloy to be made into a glass by quenching from the liquid state.<sup>4,5</sup>

Au and Si are important for technological applications, as gold is often used to make electrical contacts to semiconductor devices,<sup>6</sup> and the Au-Si eutectic alloy can be used for bonding in microelectromechanical systems.<sup>7,8</sup> Au-Si and Au-Ge eutectic alloys are also used as a catalyst for manufacturing Si and Ge nanowires, via a vapor-liquid-solid or vapor-solid-solid mechanism, for applications in nanotechnology.<sup>9–13</sup> The surface of the molten Au-Si eutectic alloy has received attention owing to the observation by x-ray reflectivity and grazing incidence x-ray-diffraction experiments of enhanced layering at the liquid surface.<sup>14,15</sup> Unlike most liquid metals and alloys, where the decay of layering order below the liquid surface is exponential and has a range (two to three atomic diameters) comparable to the correlation length of the bulk liquid,<sup>16</sup> the surface of  $\text{Au}_{0.82}\text{Si}_{0.18}$  forms a two-dimensional crystalline phase below which there are six to seven atomic layers that are liquid in a lateral direction but well defined in a direction normal to the surface, leading to a reflectivity peak that is more than an order of magnitude more intense than for other metallic liquids that have been investigated. The surface region is Si-rich relative to the bulk composition, and the surface layer undergoes a first order solid-solid phase transition at 371 °C between a low-temperature bilayer and a high-temperature monolayer phase.<sup>17</sup> Several of these observations have been confirmed in other work,<sup>18</sup> although there is a question regarding the role played by silica impurities.<sup>19</sup> The presence

of a substrate can enhance supercooling in Au-Si eutectic droplets, that is, a suitably chosen wall can inhibit freezing of the liquid phase.<sup>20,21</sup> Nearly free-standing nanometer-sized drops of the eutectic Au-Ge liquid are reported to crystallize via a mechanism that avoids nucleation in the drop center but proceeds via faceting of the supercooled liquid surface, which acts as a precursor to surface-induced crystallization.<sup>22</sup> By comparison, x-ray reflectivity and grazing incidence x-ray-diffraction experiments on the eutectic alloy  $\text{Ag}_{0.72}\text{Ge}_{0.28}$  do not show evidence of the surface freezing and surface-induced order observed for the Au-Si eutectic.<sup>16</sup>

The purpose of this paper is to use neutron diffraction to study the bulk structure of three liquid alloys at or near the eutectic composition, namely  $\text{Au}_{0.81}\text{Si}_{0.19}$ ,  $\text{Au}_{0.72}\text{Ge}_{0.28}$ , and  $\text{Ag}_{0.74}\text{Ge}_{0.26}$ . The experiments were done using a single incident neutron energy with the diffractometer D4c (Ref. 23) at the reactor source of the Institut Laue-Langevin (ILL) to avoid the neutron absorption resonances of <sup>197</sup>Au and <sup>109</sup>Ag at 4.890(2) and 5.19(1) eV, respectively.<sup>24</sup> At present, it is not possible to accurately account for the effect of these resonances on the diffraction pattern measured using time-of-flight methods at a pulsed neutron source. The new experiments complement those recently obtained by using high-energy x-ray diffraction<sup>25–27</sup> since there is a contrast between the neutron and x-ray scattering lengths (or form factors) for the constituent species of a given alloy. The results provide data that can be used to assist in developing realistic models of these fascinating eutectic systems.<sup>28,29</sup> In addition, the decay of the pair distribution functions in real space for a variety of metallic glasses has been interpreted in terms of a packing of structural units, which leads to a fractal network with a dimension of 2.31.<sup>30</sup> It is therefore of interest to investigate the extent to which liquid metallic alloys can be described within this framework, and, indeed, to examine whether the decay of the pair distribution functions can in fact be described by using the results obtained from simple theory.<sup>31–33</sup> The latter were not considered in the work

of Ma *et al.*,<sup>30</sup> although they have been used with some success to describe the decay of the partial pair distribution functions for a variety of systems, including binary mixtures of hard spheres<sup>34</sup> and binary network-forming glasses.<sup>33,35–39</sup> Additionally, in simple theories of dense binary *A-B* liquids at a liquid-vapor or wall-liquid interface, the asymptotic behavior of the single-particle liquid-density profiles  $\rho_A(r)$  and  $\rho_B(r)$  is described by exponentially damped oscillatory functions where the decay length and wavelength of the oscillatory decay are common to both species and take the same values as for the asymptotic decay of the bulk liquid partial pair distribution functions  $r[g_{\alpha\beta}(r) - 1]$ .<sup>31,40,41</sup> It is useful, therefore, to investigate the decay of the bulk liquid pair distribution functions for comparison with the density profiles obtained for inhomogeneous liquids.<sup>14–16</sup>

The paper is organized as follows. The essential theory required to understand the diffraction results is described in Sec. II, and the experimental details are outlined in Sec. III. The results are presented in Sec. IV, where they are compared with those obtained from previous diffraction experiments. In Sec. V, the asymptotic decay of the pair distribution functions in real space is characterized and the results are compared with those expected from the fractal model proposed by Ma *et al.*<sup>30</sup> and from the predictions of a simple theory based on the Ornstein-Zernike equations.<sup>31–33</sup> Finally, the conclusions are summarized in Sec. VI.

## II. THEORY

In a neutron-diffraction experiment on a liquid binary eutectic alloy, the scattered intensity containing structural information can be represented by the total structure factor<sup>42</sup>

$$F_N(k) = \sum_{\alpha=1}^n \sum_{\beta=1}^n c_{\alpha} c_{\beta} b_{\alpha} b_{\beta} [S_{\alpha\beta}(k) - 1], \quad (1)$$

where  $\alpha$  and  $\beta$  denote the chemical species,  $n = 2$  is the number of different chemical species,  $c_{\alpha}$  and  $b_{\alpha}$  represent the atomic fraction and bound coherent scattering length of chemical species  $\alpha$  respectively, and  $S_{\alpha\beta}(k)$  is a Faber-Ziman<sup>43</sup> partial structure factor.  $k = 4\pi \sin(\theta)/\lambda$  is the magnitude of the scattering vector where  $2\theta$  is the scattering angle and  $\lambda$  is the

incident neutron wavelength.  $S_{\alpha\beta}(k)$  is related to the partial pair distribution function  $g_{\alpha\beta}(r)$  by the Fourier transform relation

$$g_{\alpha\beta}(r) - 1 = \frac{1}{2\pi^2 n_0 r} \int_0^{\infty} dk k [S_{\alpha\beta}(k) - 1] \sin(kr), \quad (2)$$

where  $n_0$  is the atomic number density and  $r$  is a distance in real space. Often the total structure factor is rewritten as

$$S_N(k) = F_N(k)/\langle b \rangle^2 + 1, \quad (3)$$

where  $\langle b \rangle = c_{\alpha} b_{\alpha} + c_{\beta} b_{\beta}$  is the mean coherent scattering length. The corresponding real-space information is provided by the total pair distribution function  $G_N(r)$ , which is obtained from the Fourier transform relation

$$G_N(r) - 1 = \frac{1}{2\pi^2 n_0 r} \int_0^{\infty} dk k [S_N(k) - 1] \sin(kr) \\ = \sum_{\alpha=1}^n \sum_{\beta=1}^n \frac{c_{\alpha} c_{\beta} b_{\alpha} b_{\beta}}{\langle b \rangle^2} [g_{\alpha\beta}(r) - 1]. \quad (4)$$

For  $r$  values smaller than the distance of closest approach between the centers of two atoms,  $g_{\alpha\beta}(r) = g_{\alpha\beta}(r = 0) = 0$  such that  $G_N(r) = G_N(r = 0) = 0$ . The coherent neutron-scattering lengths used in the data analysis are  $b(\text{Au}) = 7.63(6)$ ,  $b(\text{Ag}) = 5.922(7)$ ,  $b(\text{Si}) = 4.1491(10)$ , and  $b(\text{Ge}) = 8.185(20)$  fm.<sup>44</sup>

In an x-ray-diffraction experiment, Eqs. (1), (3), and (4) remain valid provided that each  $b_{\alpha}$  is replaced by the corresponding  $k$ -dependent x-ray form factor  $f_{\alpha}(k)$  such that Eq. (3) becomes  $S_X(k) = F_X(k)/|\langle f(k) \rangle|^2 + 1$ , where the average x-ray form factor  $\langle f(k) \rangle = c_{\alpha} f_{\alpha}(k) + c_{\beta} f_{\beta}(k)$ .<sup>42</sup> The relative weighting factors for the partial structure factors in the expressions for  $S_N(k)$  and  $S_X(k)$  are listed in Table I for the investigated Au-Si, Au-Ge, and Ag-Ge alloys.

## III. EXPERIMENTAL

The alloys were prepared from Au (99.995%), Ag (99.5+%), Ge (99.9999%), and Si (99.9999%) by weighing appropriate amounts of the elements, sealing them under vacuum in a silica ampoule, and heating in a furnace for 3–4 h at a temperature up to 1000 °C while occasionally inverting the ampoule. Each sample was cooled by quenching in water. The alloys thus made were recast into billets of 3-mm diameter and then sealed under a vacuum of  $10^{-5}$  torr in silica ampoules of 4-mm inner diameter and 1-mm wall thickness ready for the

TABLE I. The weighting of the individual partial structure factors in the total structure factor measured by using neutron diffraction,  $S_N(k)$ , or x-ray diffraction,  $S_X(k)$ , in an experiment on liquid  $\text{Au}_{0.81}\text{Si}_{0.19}$ ,  $\text{Au}_{0.72}\text{Ge}_{0.28}$ , or  $\text{Ag}_{0.74}\text{Ge}_{0.26}$ .

Alloy	Pair correlation	Neutron diffraction (%)	X-ray diffraction at $k = 0$ (%)
$\text{Au}_{0.81}\text{Si}_{0.19}$	Au-Au	78.6	92.2
	Au-Si	20.1	7.7
	Si-Si	1.3	0.1
$\text{Au}_{0.72}\text{Ge}_{0.28}$	Au-Au	49.8	74.6
	Au-Ge	41.5	23.5
	Ge-Ge	8.7	1.9
$\text{Ag}_{0.74}\text{Ge}_{0.26}$	Ag-Ag	45.3	65.1
	Ag-Ge	44.0	31.2
	Ge-Ge	10.7	3.7

neutron-diffraction experiments. The latter were made using the D4c instrument<sup>23</sup> at the ILL with an incident wavelength of 0.4963(1) Å for the molten Au<sub>0.81</sub>Si<sub>0.19</sub> alloy or 0.4967(1) Å for the molten Au<sub>0.72</sub>Ge<sub>0.28</sub> and Ag<sub>0.74</sub>Ge<sub>0.26</sub> alloys. A vanadium furnace was used with a heating element of 17-mm diameter and 0.1-mm wall thickness together with a heat shield of 25-mm diameter and 0.04-mm wall thickness. Diffraction patterns were taken at a temperature just above the melting point, that is, at 392(2) °C for Au<sub>0.81</sub>Si<sub>0.19</sub>, 393(2) °C for Au<sub>0.72</sub>Ge<sub>0.28</sub>, and 703(2) °C for Ag<sub>0.74</sub>Ge<sub>0.26</sub> for the sample in its container in the furnace, for an empty container in the furnace, and for the empty furnace. Diffraction patterns were also taken at room temperature for the empty furnace, for a cylindrical vanadium rod of diameter 6.37(1) mm in the furnace for normalization purposes, and for a bar of neutron-absorbing <sup>10</sup>B<sub>4</sub>C of dimensions comparable to the sample in the furnace to account for the effect of the sample's attenuation on the background signal at small scattering angles.<sup>45</sup> Each complete diffraction pattern was built up from the intensities measured for the different detector groups. These intensities were saved at regular intervals to check the stability of the sample and instrument.<sup>46</sup>

The mass density of the liquid Au<sub>0.81</sub>Si<sub>0.19</sub>, Au<sub>0.72</sub>Ge<sub>0.28</sub>, and Ag<sub>0.74</sub>Ge<sub>0.26</sub> alloys was first estimated from the densities of the pure components by using Vegard's law. These densities were used as starting points for analyzing the x-ray-diffraction data of Refs. 25–27. The density was then adjusted and the analysis repeated until the  $S_X(k)$  function measured for an alloy was in agreement with the back Fourier transform of the corresponding  $G_X(r)$  function after the small  $r$  oscillations were set to the  $G_X(r = 0) = 0$  limit. The number densities obtained from this method are 0.0573, 0.0555, and 0.0555 Å<sup>-3</sup> for liquid Au<sub>0.81</sub>Si<sub>0.19</sub>, Au<sub>0.72</sub>Ge<sub>0.28</sub>, and Ag<sub>0.74</sub>Ge<sub>0.26</sub>, respectively. The corresponding mass densities are listed in Table II, where they are compared to the values measured for the crystalline alloys by using Archimedes' principle. The comparison shows that the liquid densities are about 2% higher than those of the corresponding crystalline materials. This is consistent with the results of Waghorne *et al.*,<sup>47</sup> who estimated that Au<sub>0.815</sub>Si<sub>0.185</sub> and Au<sub>0.75</sub>Ge<sub>0.25</sub> contract by 1%–2% and 5% on melting, respectively. For Au<sub>0.81</sub>Si<sub>0.19</sub>, the number density of the liquid is about 2% higher than for amorphous films of Au<sub>0.80</sub>Si<sub>0.20</sub> prepared by vapor deposition.<sup>48</sup> The effect of expansion upon freezing for the Au<sub>0.72</sub>Ge<sub>0.28</sub> alloy was observed at the end of our neutron-diffraction experiment as the sample broke the silica ampoule.

The absorption cross sections for Si and Ge used in the data analysis were taken from Ref. 44, while those for Au

TABLE II. The mass density of crystalline and liquid Au<sub>0.81</sub>Si<sub>0.19</sub>, Au<sub>0.72</sub>Ge<sub>0.28</sub>, and Ag<sub>0.74</sub>Ge<sub>0.26</sub> as measured by using Archimedes' principle and as estimated from the high-energy x-ray-diffraction experiments of Refs. 25–27, respectively.

Alloy	Density (g cm <sup>-3</sup> )	
	Crystal	Liquid
Au <sub>0.81</sub> Si <sub>0.19</sub>	15.43(1)	15.688
Au <sub>0.72</sub> Ge <sub>0.28</sub>	14.594(6)	14.944
Ag <sub>0.74</sub> Ge <sub>0.26</sub>	8.960(4)	9.097

and Ag were obtained from the Monte Carlo N-Particle (MCNP) library in the Korea Atomic Energy Research Institute (KAERI) database,<sup>49</sup> which gives values of 30.9 and 18.9 barns, respectively, for neutrons with an incident wavelength of 0.5 Å. The neutron-diffraction data were carefully corrected to yield the total structure factor for each sample and the usual self-consistency checks were performed.<sup>50,51</sup>

#### IV. RESULTS

The measured total structure factors  $S_N(k)$  for the eutectic alloys are shown in Fig. 1. Each function has a relatively sharp principal peak at a scattering vector  $k_{PP}$  of 2.72(2), 2.71(2), and 2.69(2) Å<sup>-1</sup> with a half-width at half-maximum of 0.25(2), 0.30(2), and 0.26(2) Å<sup>-1</sup> for liquid Au<sub>0.81</sub>Si<sub>0.19</sub>, Au<sub>0.72</sub>Ge<sub>0.28</sub>, and Ag<sub>0.74</sub>Ge<sub>0.26</sub>, respectively. We refer to this feature in  $S_N(k)$  as the principal peak to avoid confusion with a peak at  $\simeq 1$ –1.5 Å<sup>-1</sup> that commonly occurs in network glass-forming systems and which is referred to as a prepeak

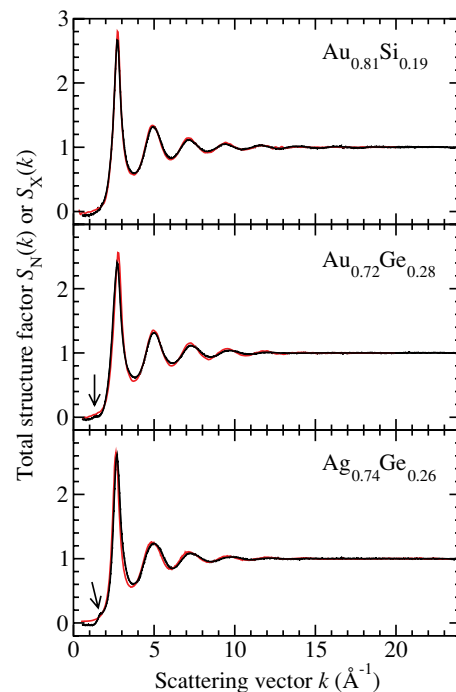


FIG. 1. (Color online) The total structure factors  $S_N(k)$  measured by using neutron diffraction for liquid Au<sub>0.81</sub>Si<sub>0.19</sub> at 392(2) °C, Au<sub>0.72</sub>Ge<sub>0.28</sub> at 393(2) °C, and Ag<sub>0.74</sub>Ge<sub>0.26</sub> at 703(2) °C. The vertical bars represent the measured data points with statistical errors, and the solid dark (black) curves are the back Fourier transforms of the corresponding real-space functions  $G_N(r)$  given by the solid dark (black) curves in Fig. 2, where the unphysical oscillations at  $r$  values smaller than the distance of closest approach between the centers of two atoms are set to the calculated  $G_N(r = 0) = 0$  limit. For all of the functions, the back Fourier transforms are indistinguishable from the data points at most  $k$  values and the error bars on these data points are smaller than the line thickness. The arrows point to small prepeaks in  $S_N(k)$  at  $\simeq 1.3$  and  $1.6$  Å<sup>-1</sup> for the Au-Ge and Ag-Ge alloys, respectively. The solid light (red) curves give the total structure factors  $S_X(k)$  measured by using high-energy x-ray diffraction for liquid Au<sub>0.81</sub>Si<sub>0.19</sub> at 380 °C (Refs. 26 and 27), Au<sub>0.72</sub>Ge<sub>0.28</sub> at 380 °C (Refs. 26 and 27), and Ag<sub>0.74</sub>Ge<sub>0.26</sub> at 700 °C (Ref. 25).

or first sharp diffraction peak.<sup>52</sup> The results are compared to the total structure factors  $S_X(k)$  for these alloys as measured by using high-energy (113.26 or 181.00 keV) x-ray diffraction in transmission geometry by Takeda and co-workers.<sup>25–27</sup> The latter are comparable to the neutron-diffraction results, and each shows a relatively sharp principal peak at a position  $k_{PP}$  of 2.73(2)  $\text{\AA}^{-1}$  for  $\text{Au}_{0.81}\text{Si}_{0.19}$  at 380 °C, 2.77(3)  $\text{\AA}^{-1}$  for  $\text{Au}_{0.72}\text{Ge}_{0.28}$  at 380 °C, and 2.63(2)  $\text{\AA}^{-1}$  for  $\text{Ag}_{0.74}\text{Ge}_{0.26}$  at 700 °C. The  $S_N(k)$  functions for liquid  $\text{Au}_{0.72}\text{Ge}_{0.28}$  and  $\text{Ag}_{0.74}\text{Ge}_{0.26}$  also show prepeaks at 1.3(2) and 1.6(3)  $\text{\AA}^{-1}$ , respectively. A prepeak for the Au-Ge alloy at 1.35(10)  $\text{\AA}^{-1}$  which survives with temperature increasing to 1000 °C was observed in the x-ray-diffraction work of Hoyer and Jödicke,<sup>53</sup> who used reflection ( $\theta$ - $\theta$ ) geometry with low-energy x-rays (17.48 keV), and was taken to be a signature of medium-range order caused by the formation of heteroatomic clusters. This feature was not, however, found in more recent high-energy x-ray-diffraction experiments,<sup>26,27</sup> which were made in transmission geometry using x-rays of energy 181.00 keV with a large penetration depth. The discrepancy may arise from the greater sensitivity of the former to surface effects.

The reciprocal space functions of the present work were extrapolated to  $k = 0$  by assuming that  $S_N(k) \propto k^2$  at small  $k$  values.<sup>36</sup> They were then spline-fitted and Fourier-transformed to give the real-space functions  $G_N(r)$  shown in Fig. 2. In these

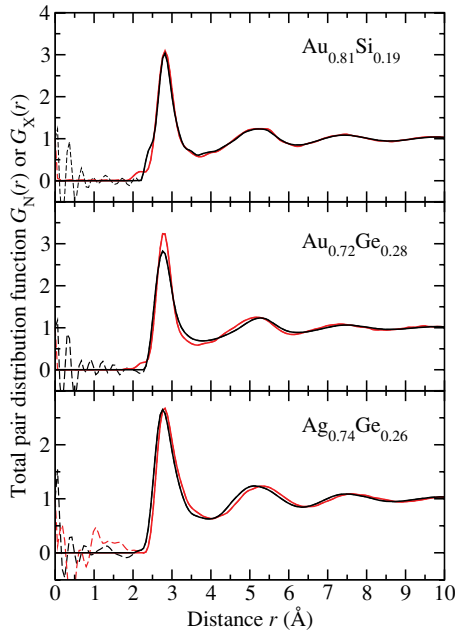


FIG. 2. (Color online) The total pair distribution functions  $G_N(r)$  [solid dark (black) curves] for liquid  $\text{Au}_{0.81}\text{Si}_{0.19}$  at 392(2) °C,  $\text{Au}_{0.72}\text{Ge}_{0.28}$  at 393(2) °C, and  $\text{Ag}_{0.74}\text{Ge}_{0.26}$  at 703(2) °C, as obtained by spline fitting and Fourier transforming the corresponding  $S_N(k)$  functions shown in Fig. 1, after setting the small  $r$  oscillations to the appropriate  $G_N(r = 0)$  limiting value. The data are compared to the  $G_X(r)$  functions [solid light (red) curves] as measured by using high-energy x-ray diffraction for liquid  $\text{Au}_{0.81}\text{Si}_{0.19}$  at 380 °C (Refs. 26 and 27),  $\text{Au}_{0.72}\text{Ge}_{0.28}$  at 380 °C (Refs. 26 and 27), and  $\text{Ag}_{0.74}\text{Ge}_{0.26}$  at 700 °C (Ref. 25). The broken dark (black) and broken light (red) curves show the extent of the unphysical small  $r$  oscillations in  $G_N(r)$  and  $G_X(r)$ , respectively.

figures, the results are compared with the  $G_X(r)$  functions measured by high-energy x-ray diffraction.<sup>25–27</sup>

### A. Liquid $\text{Au}_{0.81}\text{Si}_{0.19}$

The  $G_N(r)$  and  $G_X(r)$  functions for liquid  $\text{Au}_{0.81}\text{Si}_{0.19}$  are very similar, with the exception of a shoulder that appears on  $G_N(r)$  at  $\simeq 2.4$  Å. The first peak occurs at 2.83(2) Å in  $G_N(r)$  and at 2.82(2) Å in  $G_X(r)$  and is attributed, on the basis of the weighting factors given in Table I, to the nearest-neighbor Au-Au distance. Other x-ray-diffraction experiments on the liquid give a nearest-neighbor distance of  $\sim 2.85$  Å.<sup>47</sup> The nearest-neighbor distance in liquid gold is  $\simeq 2.72(2)$  Å at 1150 °C.<sup>26,27</sup> In liquid silicon,<sup>54,55</sup> the Si-Si bond distance is 2.44–2.48 Å, and in crystals like  $\text{YbAuSi}$ ,<sup>56</sup>  $\text{CaAu}_{1.208}\text{Si}_{0.792}$ ,<sup>56</sup> and  $\text{CeAu}_4\text{Si}_2$ ,<sup>57,58</sup> the nearest-neighbor Si-Si and Au-Si distances are 2.19–2.64 and 2.48–2.64 Å, respectively. Hence, by considering the weighting factors listed in Table I, the absence of a shoulder in  $G_X(r)$  at 2.4 Å can be attributed to the relatively small weighting of the Au-Si and Si-Si pair correlation functions while the appearance of this shoulder in  $G_N(r)$  can be attributed to Au-Si pair correlations. As shown in Fig. 3, the measured  $G_N(r)$  function is in good accord with the results obtained from the first-principles molecular-dynamics work of Pasturel *et al.*<sup>29</sup>

The results are consistent with thermodynamic measurements that point to the preferred association of unlike atoms in the liquid eutectic alloy.<sup>5</sup> The results are also consistent with the first-principles molecular-dynamics work of Lee and Hwang<sup>28</sup> on several amorphous Au-Si alloys, which suggest that there is a clustering of Au around Si atoms for Au-rich

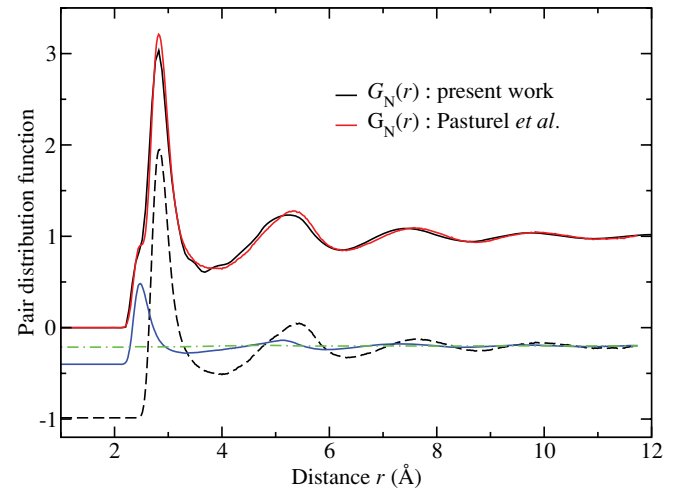


FIG. 3. (Color online) Comparison between the total pair distribution function  $G_N(r)$  for liquid  $\text{Au}_{0.81}\text{Si}_{0.19}$  as measured at 392(2) °C in the present work [solid dark (black) curve] and as calculated at 427 °C in the first-principles molecular-dynamics work of Pasturel *et al.*<sup>29</sup> [solid light (red) curve] wherein the number density was 0.056  $\text{\AA}^{-3}$ . The  $G_N(r)$  function for the latter was obtained by summing the weighted Au-Au [broken (black) curve], Au-Si [solid (blue) curve], and Si-Si [chained (green) curve] partial pair distribution functions taken from Ref. 29, where the weighting factors on the  $g_{\alpha\beta}(r) - 1$  functions are given by Eq. (4). The weighted  $g_{\alpha\beta}(r) - 1$  functions are displaced downward by 0.2 units for clarity of presentation.

systems such that the Si atoms are more or less evenly distributed. The calculations show the formation of Si-centered tricapped trigonal prism Kasper polyhedra with an Au-Si bond distance of  $\approx 2.4$  Å (the associated Au-Au distance is expected to be<sup>59</sup>  $2.4/0.86 = 2.79$  Å). The Si-Au coordination number of 9 compares to a mean value of  $\approx 10$  found from reverse Monte Carlo (RMC) models of the x-ray-diffraction data taken for liquid  $\text{Au}_{0.81}\text{Si}_{0.19}$  at various temperatures.<sup>26,27</sup> In Si-rich  $\text{Au}_x\text{Si}_{1-x}$  ( $0.14 \leq x \leq 0.34$ ) amorphous alloys prepared by vapor deposition, an Au-Au distance of 2.82–2.83 Å with a Si-Si or Au-Si distance of 2.40–2.42 Å was reported.<sup>60</sup>

### B. Liquid $\text{Au}_{0.72}\text{Ge}_{0.28}$

The  $G_N(r)$  and  $G_X(r)$  functions for liquid  $\text{Au}_{0.72}\text{Ge}_{0.28}$  show discrepancies that can be attributed to the different weighting factors for the partial pair correlation functions (see Table I). The first peak in  $G_N(r)$  at 2.76(2) Å, where Au-Au and Au-Ge pair correlations dominate the diffraction pattern and have comparable weighting factors, is shifted to small  $r$  relative to the first peak in  $G_X(r)$  at 2.79(2) Å, where the Au-Au pair correlations dominate the diffraction pattern. The first peak shift for the latter can therefore be attributed to a larger contribution from Au-Au correlations. Diffraction and extended x-ray-absorption fine-structure (EXAFS) experiments on liquid germanium<sup>50,61,62</sup> give a Ge-Ge bond distance of 2.62–2.66 Å while the nearest-neighbor distance in crystalline  $\text{Au}_{0.8}\text{Ge}_{0.2}$  is 2.85–2.86 Å at high pressure.<sup>63</sup> The nearest-neighbor distance in liquid gold is  $\approx 2.72(2)$  Å at 1150 °C,<sup>26,27</sup> and RMC models of liquid  $\text{Au}_{0.72}\text{Ge}_{0.28}$  at 380 °C point to a mean Ge-Au coordination number of  $\approx 8$ .<sup>26,27</sup> Previous diffraction experiments used reflection ( $\theta$ - $\theta$ ) geometry and low-energy x-rays (8.05 or 17.48 keV), making them more sensitive to surface effects, and give a somewhat larger nearest-neighbor distance of 2.85 Å for liquid  $\text{Au}_{0.72}\text{Ge}_{0.28}$  (Ref. 53) and 2.87 Å for liquid  $\text{Au}_{75}\text{Ge}_{25}$ .<sup>47</sup>

### C. Liquid $\text{Ag}_{0.74}\text{Ge}_{0.26}$

The  $G_N(r)$  and  $G_X(r)$  functions for liquid  $\text{Ag}_{0.74}\text{Ge}_{0.26}$  give first peak positions of 2.77(2) and 2.81(2) Å, respectively. As shown by Table I, the weighting factors for the partial pair correlation functions follow the same trend as for  $\text{Au}_{0.72}\text{Ge}_{0.28}$ , that is, the Ag-Ag and Ag-Ge pair correlations dominate  $G_N(r)$  and have comparable weighting factors, whereas the Ag-Ag pair correlations dominate  $G_X(r)$ .

The structure of the liquid eutectic alloy  $\text{Ag}_{0.76}\text{Ge}_{0.24}$  at 850 °C was measured by Bellissent-Funel *et al.*<sup>64</sup> using the method of silver isotope substitution in neutron diffraction. The experiment was done using the D4 diffractometer at the ILL (an earlier version of D4c), but the limitations of this instrument at the time meant that the partial structure factors were measured up to a relatively short maximum  $k$  value of  $12 \text{ \AA}^{-1}$ . The measured nearest-neighbor Ag-Ag, Ag-Ge, and Ge-Ge distances are 2.92, 2.66, and 3.12 Å, respectively. In Fig. 4, a comparison is made between the  $G_N(r)$  function obtained by Fourier transforming the  $S_N(k)$  function measured for liquid  $\text{Ag}_{0.74}\text{Ge}_{0.26}$  in the present work, after truncating at  $k = 12 \text{ \AA}^{-1}$ , and the results of Ref. 64 for liquid  $\text{Ag}_{0.76}\text{Ge}_{0.24}$ . The total pair distribution function for

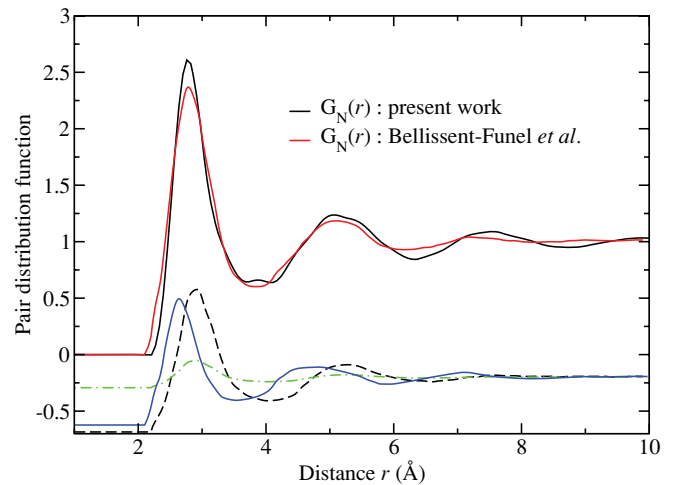


FIG. 4. (Color online) Comparison between the total pair distribution functions  $G_N(r)$  for liquid  $\text{Ag}_{0.74}\text{Ge}_{0.26}$  at 703(2) °C from the present work [solid dark (black) curve] and liquid  $\text{Ag}_{0.76}\text{Ge}_{0.24}$  at 850 °C from the work of Bellissent-Funel *et al.*<sup>64</sup> [solid light (red) curve]. The  $G_N(r)$  function for  $\text{Ag}_{0.74}\text{Ge}_{0.26}$  was obtained by truncating the  $S_N(k)$  function shown in Fig. 1 at  $12 \text{ \AA}^{-1}$ , Fourier transforming, and setting the small  $r$  oscillations to the  $G_N(r = 0)$  limiting value. The  $G_N(r)$  function for  $\text{Ag}_{0.76}\text{Ge}_{0.24}$  was obtained by summing the weighted Ag-Ag [broken (black) curve], Ag-Ge [solid (blue) curve], and Ge-Ge [chained (green) curve] partial pair distribution functions digitized from Ref. 64, where the weighting factors on the  $g_{\alpha\beta}(r) - 1$  functions are given by Eq. (4). The weighted  $g_{\alpha\beta}(r) - 1$  functions are displaced downward by 0.2 units for clarity of presentation.

the latter was obtained by adding the weighted  $g_{\alpha\beta}(r) - 1$  functions according to Eq. (4), using  $c_{\text{Ag}} = 0.76$ ,  $c_{\text{Ge}} = 0.24$ , and the scattering lengths taken from Sears.<sup>44</sup> The  $G_N(r)$  functions for the  $\text{Ag}_{0.74}\text{Ge}_{0.26}$  and  $\text{Ag}_{0.76}\text{Ge}_{0.24}$  liquids show comparable features and, in the region of the first peak, there is considerable overlap between the individual pair distribution functions. We note that, while discrepancies between the  $G_N(r)$  functions measured in the present work and Ref. 64 are expected from the different compositions and temperatures, the partial structure factors from Ref. 64 were extracted from the measured diffraction patterns by using scattering lengths for the Ag isotopes that have since been revised (see Ref. 44).

## V. DISCUSSION

Two approaches will be considered for the asymptotic behavior of the total pair distribution functions in real space. The first is based on a fractal model for the structure that has been proposed by Ma *et al.*<sup>30</sup> The second is based on a pole analysis of the Ornstein-Zernike equations for pair interaction potentials<sup>31,32</sup> and includes models for mixtures of hard spheres.<sup>41,65</sup>

### A. Fractal approach to the decay of the pair distribution functions

If it is assumed that the material is made from clusters of structural units that show a degree of self-similarity or scale

invariance, then the mass of a cluster increases with its linear dimension  $r$  according to the relation<sup>66</sup>

$$M(r) \propto r^{D_f}, \quad D_f < D, \quad (5)$$

where  $D_f$  is the fractal dimension and  $D$  is the embedding dimension. For a uniform local density,  $M(r) \propto V(r)$ , where  $V(r)$  is the volume of a cluster such that  $r \propto V(r)^{1/D_f}$ . Ma *et al.*<sup>30</sup> take  $V(r)$  to be the atomic volume  $v$  calculated from the measured density and assume that the principal peak position  $k_{pp}$  in  $S_X(k)$  or  $S_N(k)$  is proportional to the reciprocal of the linear dimension  $r$  such that  $k_{pp} \propto v^{-1/D_f}$  or

$$\ln k_{pp} = \ln a - \frac{\ln v}{D_f}, \quad (6)$$

where  $a$  is the constant of proportionality. As shown by Fig. 5(a), the data for a wide variety of glassy metals plotted according to Eq. (6) give a gradient of  $-0.433(6)$  as opposed to  $-1/3$ . The latter value is expected, for example, for a crystalline metal<sup>30</sup> or for a hard-sphere model of the liquid structure factor since, for a given packing fraction  $\eta = \pi\sigma^3/6v$ , where  $\sigma$  is the hard-sphere diameter,  $k_{pp}\sigma = \text{const}$  such that  $k_{pp} \propto v^{-1/3}$ .<sup>67</sup> A fractal dimension  $D_f = 1/0.433 = 2.31$  was thereby deduced for metallic glasses. Following Ma *et al.*,<sup>30</sup> the asymptotic decay of a total pair distribution function is then modeled by using

$$r^{D'} [G_N(r) - 1] \simeq A \exp(-a_0 r) \cos(a_1 r - \phi), \quad (7)$$

where  $D' \equiv D - D_f = 0.69$ ,  $A$  is an amplitude, and  $\phi$  is a phase. The oscillatory term was included to modify an expression previously used to model the small-angle neutron-scattering data measured for silica particle aggregates, where  $\xi = a_0^{-1}$  is a cutoff length chosen to ensure that the aggregates (or clusters) are not infinite in extent.<sup>66</sup> The wavelength of the oscillatory term is  $2\pi/a_1$ , where  $a_1$  is identified with  $k_{pp}$ .

As shown in Fig. 5(a), the densities measured for liquid  $\text{Au}_{0.81}\text{Si}_{0.19}$ ,  $\text{Au}_{0.72}\text{Ge}_{0.28}$ , and  $\text{Ag}_{0.74}\text{Ge}_{0.26}$  in the present work

and for glassy  $\text{Au}_{0.80}\text{Si}_{0.20}$  in the work by Mangin *et al.*<sup>48</sup> are consistent with the results obtained for many metallic glasses. Thus, although a fractal model will not be valid for a uniform liquid, the neutron-diffraction results for the molten alloys were analyzed according to Eq. (7).

### B. Ornstein-Zernike approach to the decay of the pair distribution functions

Evans and co-workers<sup>31,32</sup> made a pole analysis of the Ornstein-Zernike equations for binary systems in which the particle interactions are pairwise additive and are described by either short-ranged repulsive potentials or short-ranged repulsive plus long-ranged Coulomb potentials. If the particle density is sufficiently high, the asymptotic behavior of each partial pair distribution function is described by the relation

$$r[g_{\alpha\beta}(r) - 1] = 2|\mathcal{A}_{\alpha\beta}| \exp(-a_0 r) \cos(a_1 r - \theta_{\alpha\beta}), \quad (8)$$

where each function has a common decay length given by  $a_0^{-1}$  and a common wavelength of oscillation given by  $2\pi/a_1$ . The amplitudes are related by  $|\mathcal{A}_{\alpha\alpha}||\mathcal{A}_{\beta\beta}| = |\mathcal{A}_{\alpha\beta}|^2$  and the phases are related by  $\theta_{\alpha\alpha} + \theta_{\beta\beta} = 2\theta_{\alpha\beta}$ . By using the definition of the total pair distribution function given by Eq. (4), it follows that

$$r[G_N(r) - 1] = 2|\mathcal{A}| \exp(-a_0 r) \cos(a_1 r - \theta), \quad (9)$$

where  $\mathcal{A} = (c_\alpha b_\alpha \mathcal{A}_{\alpha\alpha}^{1/2} + c_\beta b_\beta \mathcal{A}_{\beta\beta}^{1/2})^2 / \langle b \rangle^2 \equiv |\mathcal{A}| \exp(-i\theta)$ ,  $\mathcal{A}_{\alpha\alpha} = |\mathcal{A}_{\alpha\alpha}| \exp(-i\theta_{\alpha\alpha})$ ,  $\mathcal{A}_{\beta\beta} = |\mathcal{A}_{\beta\beta}| \exp(-i\theta_{\beta\beta})$ ,  $i = \sqrt{-1}$ , and  $\theta$  is a phase. By inspection, the only significant difference between Eqs. (7) and (9) is the power of  $r$  used to weight  $G_N(r) - 1$ .

### C. Description of the asymptotic decay

The measured  $r^{D'} [G_N(r) - 1]$  and  $r[G_N(r) - 1]$  functions for the liquid Au-Si, Au-Ge, and Ag-Ge alloys were fitted at large  $r$  values by using Eqs. (7) and (9), respectively. The

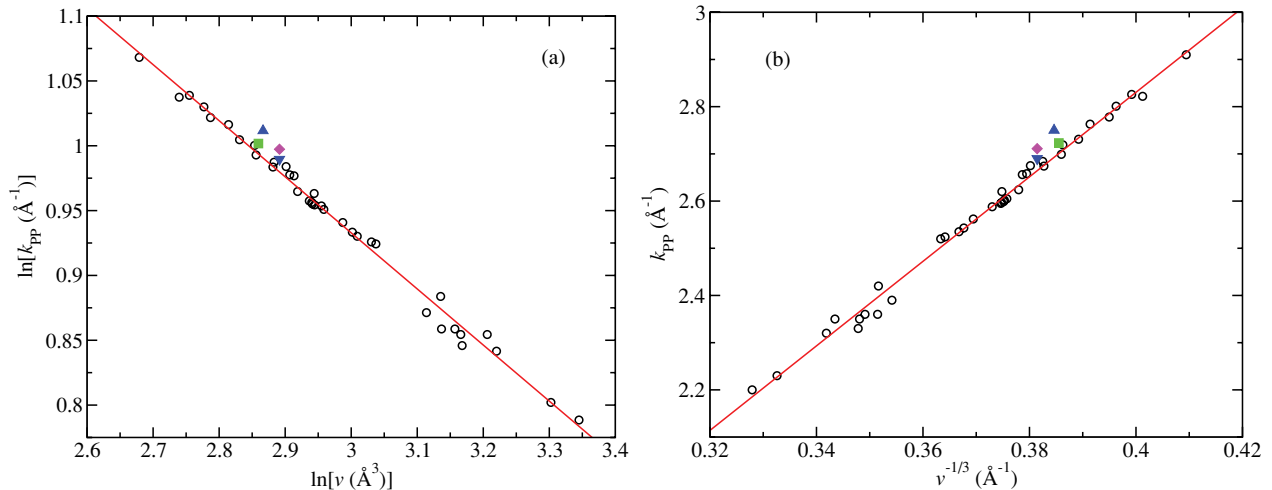


FIG. 5. (Color online) Plots of (a)  $\ln k_{pp}$  vs  $\ln v$  and (b)  $k_{pp}$  vs  $v^{-1/3}$  for various metallic glasses (open circles) as taken from Ma *et al.*<sup>30</sup> The solid (red) curves are straight-line fits to the data and give a gradient and goodness-of-fit parameter  $R^2$  of (a)  $-0.433(6)$  and  $0.9922$  or (b)  $8.95(13)$  and  $0.9926$ , respectively. Also shown are the data points for molten  $\text{Au}_{0.81}\text{Si}_{0.19}$  at  $392(2)^\circ\text{C}$  [(green) ■],  $\text{Au}_{0.72}\text{Ge}_{0.28}$  at  $393(2)^\circ\text{C}$  [(magenta) ◆], and  $\text{Ag}_{0.74}\text{Ge}_{0.26}$  at  $703(2)^\circ\text{C}$  [(blue) ▼] taken from the present work, and glassy  $\text{Au}_{0.80}\text{Si}_{0.20}$  [(blue) ▲] taken from Ref. 48.

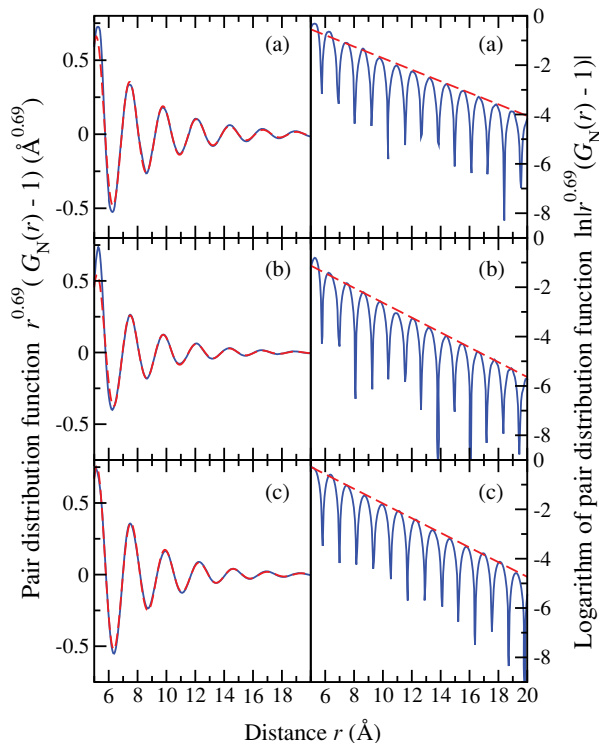


FIG. 6. (Color online) Decay of the total pair distribution functions for liquid (a)  $\text{Au}_{0.81}\text{Si}_{0.19}$  at  $392(2)^\circ\text{C}$ , (b)  $\text{Au}_{0.72}\text{Ge}_{0.28}$  at  $393(2)^\circ\text{C}$ , and (c)  $\text{Ag}_{0.74}\text{Ge}_{0.26}$  at  $703(2)^\circ\text{C}$ . In the left-hand column, the solid dark (blue) curves show plots of  $r^{D'}[G_N(r) - 1]$  vs  $r$ , and in the right-hand column the solid dark (blue) curves show plots of  $\ln|r^{D'}[G_N(r) - 1]|$  vs  $r$ , where  $D' = 0.69$ . In the left-hand column, the broken (red) curves show fits to  $r^{D'}[G_N(r) - 1]$  at large  $r$  values using Eq. (7), and in the right-hand column the broken (red) curves show straight-line fits to the maxima in  $\ln|r^{D'}[G_N(r) - 1]|$  at large  $r$  values.

maxima in the functions  $\ln|r^{D'}[G(r) - 1]|$  and  $\ln|r[G_N(r) - 1]|$  at large  $r$  values were also fitted with straight lines to obtain separate values for  $a_0$ . The fits are shown in Figs. 6 and 7, and several of the fitted parameters are summarized in Table III. The quality of a fit is measured by  $R^2 \equiv 1 - \sum_i (y_i - y_{\text{fit},i})^2 / \sum_i (y_i - \bar{y})^2$ , where the summations extend over the fitted range of data points,  $y_i$  represents a data point,  $y_{\text{fit},i}$  represents the fitted function, and  $\bar{y}$  is the average

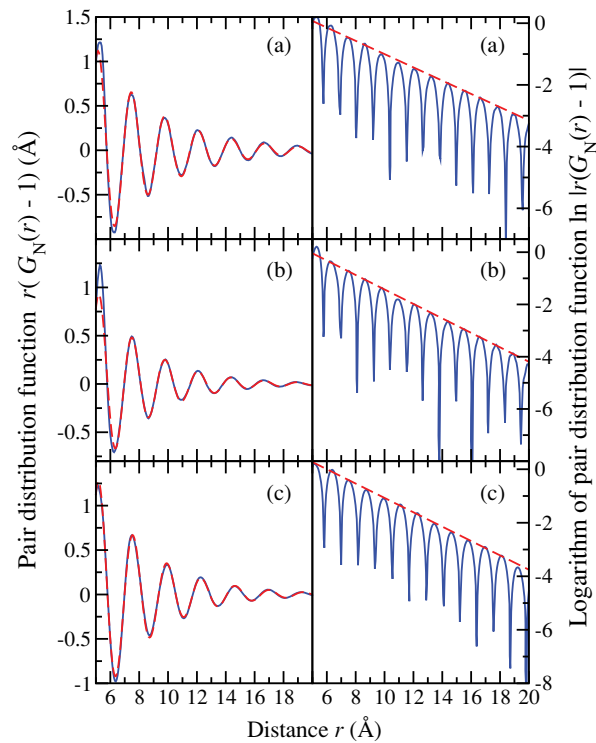


FIG. 7. (Color online) Decay of the total pair distribution functions for liquid (a)  $\text{Au}_{0.81}\text{Si}_{0.19}$  at  $392(2)^\circ\text{C}$ , (b)  $\text{Au}_{0.72}\text{Ge}_{0.28}$  at  $393(2)^\circ\text{C}$ , and (c)  $\text{Ag}_{0.74}\text{Ge}_{0.26}$  at  $703(2)^\circ\text{C}$ . In the left-hand column, the solid dark (blue) curves show plots of  $r[G_N(r) - 1]$  vs  $r$ , and in the right-hand column the solid dark (blue) curves show plots of  $\ln|r[G_N(r) - 1]|$  vs  $r$ . In the left-hand column, the broken (red) curves show fits to  $r[G_N(r) - 1]$  at large  $r$  values using Eq. (9), and in the right-hand column the broken (red) curves show straight-line fits to the maxima in  $\ln|r[G_N(r) - 1]|$  at large  $r$  values.

value of  $y_i$  for the fitted range. All of the fits for a given alloy were made over the same  $r$  space range. The minimum  $r$  value chosen for a fit is in accord with the value obtained by using the procedure outlined by Ma *et al.*,<sup>30</sup> and the maximum  $r$  value is limited by the signal-to-noise ratio.

The fractal and Ornstein-Zernike approaches for describing the asymptotic decay of the pair distribution functions give comparable fits as expected from the similarity of Eqs. (7)

TABLE III. The parameters obtained by fitting the neutron-diffraction data for liquid  $\text{Au}_{0.81}\text{Si}_{0.19}$ ,  $\text{Au}_{0.72}\text{Ge}_{0.28}$ , and  $\text{Ag}_{0.74}\text{Ge}_{0.26}$  by using Eq. (7) based on a fractal model or Eq. (9) based on a model obtained from the Ornstein-Zernike (OZ) equations. All of the fits for a given alloy were made over the same range in  $r$  space. The decay length  $a_0^{-1}$  was also obtained from a straight-line fit at large  $r$  values to the maxima in a plot of  $\ln|r^{D'}[G(r) - 1]|$  (fractal model) or  $\ln|r[G(r) - 1]|$  (OZ model) versus  $r$ .

Alloy	Range (Å)	Fractal model			OZ model			$R^2$	$a_0^a$ (Å <sup>-1</sup> )
		$a_0$ (Å <sup>-1</sup> )	$a_1$ (Å <sup>-1</sup> )	$R^2$	$a_0$ (Å <sup>-1</sup> )	$a_1$ (Å <sup>-1</sup> )	$R^2$		
Au-Si	6.26–30.56	0.270(2)	2.720(2)	0.996	0.234(2)	0.232(1)	2.721(1)	0.997	0.215(2)
Au-Ge	6.32–21.23	0.323(2)	2.745(2)	0.998	0.301(3)	0.287(2)	2.746(2)	0.998	0.277(3)
Ag-Ge	5.22–18.16	0.311(2)	2.659(2)	0.997	0.297(4)	0.273(2)	2.659(2)	0.997	0.268(3)

<sup>a</sup>From a straight-line fit to the maxima in  $\ln|r^{D'}[G(r) - 1]|$  or  $\ln|r[G(r) - 1]|$ .

and (9). For a given liquid alloy, the values of  $a_0$  and  $a_1$  obtained from the fits are comparable to the half-width at half-maximum of the principal peak in  $S_N(k)$  and to the position  $k_{pp}$  of this peak, respectively (see Sec. IV). The decay lengths  $\xi = a_0^{-1}$  obtained from the fits to the fractal model using Eq. (7) are 3.70(3), 3.10(2), and 3.22(2) Å for the liquid Au-Si, Au-Ge, and Ag-Ge alloys, respectively. These results compare with a value of  $\xi = 4.00(8)$  Å for  $Zr_{0.355}Cu_{0.645}$ , a typical metallic glass.<sup>30</sup>

#### D. Effect of the diffractometer resolution function on the decay of the pair correlation functions

The  $k$ -space resolution function of a diffractometer will lead to a finite coherence volume in real space over which correlations can be observed. In the case of a diffractometer with a Gaussian resolution function  $M(k) = \exp[-k^2/2(\Delta k)^2]/(2\pi)^{1/2}\Delta k$  of standard deviation  $\Delta k$ , the function  $G_N(r) - 1$  will be damped by a multiplicative factor  $M(r) = \exp[-(\Delta k)^2 r^2/2]$  (see Appendix C of Ref. 33). A pair distribution function analysis<sup>68</sup> of the diffraction patterns measured for powdered samples of  $CeO_2$  and  $KMgF_3$  at 90 K by using D4c with an incident neutron wavelength of 0.5 Å is consistent with an approximately Gaussian  $k$ -space resolution function with an effective standard deviation  $\Delta k \simeq 0.039$  Å<sup>-1</sup>.<sup>69</sup> This empirical result for  $\Delta k$  is compatible with an estimate based on the neutron optics of D4c operating at a wavelength of 0.5 Å and leads to a full width at half-maximum for  $M(r)$  of  $2\sqrt{2\ln 2}/\Delta k \simeq 60.4$  Å. To estimate the effect of the  $k$ -space resolution function, the measured  $r^{D_f}[G_N(r) - 1]$  and  $r[G_N(r) - 1]$  functions of Figs. 6 and 7 were divided by  $M(r)$  and the resultant functions were refitted using Eqs. (7) and (9), respectively. This led to values for  $a_1$  that are, within the experimental error, the same as those given in Table III, but to values for  $a_0$  that are reduced by 4%–9%, depending on the alloy. The effect of the finite  $k$ -space resolution function is sufficiently small that Eqs. (7) and (9) remain valid over the range of  $r$  values where oscillations are discernible in the measured total pair distribution functions.

#### E. Critique of the fractal and Ornstein-Zernike approaches

The cornerstones for the fractal model of Ma *et al.*<sup>30</sup> are (i)  $k_{pp} \propto v^{-1/D_f}$  with  $D_f \neq 3$  [see Fig. 5(a)] and (ii) the ability of Eq. (7) to account for the decay of the total pair distribution functions over a large  $r$  range. It is not, however, necessary to invoke a fractal model for the structure to account for these observations. As shown in Fig. 5(b), the available data for metallic glasses can in fact be equally well fitted by using the relation  $k_{pp} \propto v^{-1/3}$ , as expected for a three-dimensional structure. Equation (9) also accounts for the measured behavior of the total pair distribution functions for the liquid alloys over a large  $r$  range. A similar conclusion is anticipated for the glassy metals studied by Ma *et al.*<sup>30</sup> given the similarity between the equations obtained from the fractal and Ornstein-Zernike approaches. This sets a challenge to the authors of Ref. 30 to provide an analysis of their measured pair distribution functions using a standard Ornstein-Zernike approach.

The asymptotic behavior of the pair distribution functions deduced from a pole analysis of the Ornstein-Zernike relations was derived using simple pair potentials and is valid, for example, for a binary system of hard spheres.<sup>31–33</sup> This approach does not, however, take into account the effect of conduction electrons or dispersion forces—the latter lead to a power-law decay for the pair distribution functions. Further work is required to develop more realistic models for the asymptotic decay of the pair distribution functions in liquid and glassy metallic systems that go beyond an account of sphere-packing effects.

We note that unlike a model based on the Ornstein-Zernike relations, the fractal model of Ma *et al.*<sup>30</sup> does not readily lend itself to a decomposition of  $G_N(r) - 1$  into its contributions from the partial pair distribution functions. We also note that in the case of x-ray diffraction, a combination of the  $r[g_{\alpha\beta}(r) - 1]$  functions given by Eq. (8) to produce a total pair distribution function  $r[G_X(r) - 1]$  is complicated by the  $k$  dependence of the x-ray form factors that weight the  $S_{\alpha\beta}(k) - 1$  functions in the expression for  $S_X(k)$ . This leads to a convolution in real space of the Fourier transforms of the form factors and the  $r[g_{\alpha\beta}(r) - 1]$  functions (see, e.g., Appendix A of Ref. 70).

## VI. CONCLUSIONS

The structure of the molten alloys  $Au_{0.81}Si_{0.19}$ ,  $Au_{0.72}Ge_{0.28}$ , and  $Ag_{0.74}Ge_{0.26}$ , with composition at or near the eutectic, was investigated by using neutron diffraction. Small prepeaks at 1.3(2) and 1.6(3) Å<sup>-1</sup> were found in the total structure factors measured for the Au-Ge and Ag-Ge liquids, respectively. Nearest-neighbor Au-Si correlations at  $\simeq 2.4$  Å were identified for the Au-Si liquid. The large  $r$  behavior of a total pair distribution function  $r[G_N(r) - 1]$  is described by an exponentially damped oscillatory function with a decay length and wavelength of oscillation related to the half-width at half-maximum of the principal peak in the total structure factor and to the position of this peak, respectively. This type of behavior accounts for a measured function over a wide  $r$  space range extending from 5–6 Å to beyond 20 Å. There is no need to invoke the existence of a fractal network as suggested by the work of Ma *et al.*,<sup>30</sup> although the results for the liquid alloys can also be described within this framework. Atomistic models that take into account the effect of electron screening are required to examine in more detail the large  $r$  behavior of the partial pair distribution functions.

## ACKNOWLEDGMENTS

We gratefully thank Pierre Palleau (Grenoble) for help with the neutron-diffraction experiments, Phil Jones (Bath) for his glass-blowing expertise, Rob Jack (Bath) and Bob Evans (Bristol) for helpful discussions, and Alain Pasturel (Grenoble) and Noël Jakse (Grenoble) for supplying their numerical results. P.C. would like to thank the Royal Thai Government for financial support. We also thank the EPSRC for financial support and for providing its Chemical Database Service.

- \*Permanent address: Department of Material and Biological Chemistry, Faculty of Science, Yamagata University, 1-4-12 Koshirakawa, Yamagata 990-8560, Japan.
- <sup>1</sup>H. Okamoto and T. B. Massalski, *Bull. Alloy Phase Diagrams* **4**, 190 (1983).
  - <sup>2</sup>H. Okamoto and T. B. Massalski, *Bull. Alloy Phase Diagrams* **5**, 601 (1984).
  - <sup>3</sup>R. W. Olesinski and G. J. Abbaschian, *Bull. Alloy Phase Diagrams* **9**, 58 (1988).
  - <sup>4</sup>W. Klement Jr., R. H. Willens, and P. Duwez, *Nature (London)* **187**, 869 (1960).
  - <sup>5</sup>H. S. Chen and D. Turnbull, *J. Appl. Phys.* **38**, 3646 (1967).
  - <sup>6</sup>A. K. Green and E. Bauer, *J. Appl. Phys.* **47**, 1284 (1976).
  - <sup>7</sup>A.-L. Tiensuu, M. Bexell, J.-Å. Schweitz, L. Smith, and S. Johansson, *Sens. Actuators A* **45**, 227 (1994).
  - <sup>8</sup>Y. T. Cheng, L. Lin, and K. Najafi, *J. Microelectromech. Syst.* **9**, 3 (2000).
  - <sup>9</sup>J. B. Hannon, S. Kodambaka, F. M. Ross, and R. M. Tromp, *Nature (London)* **440**, 69 (2006).
  - <sup>10</sup>S. Kodambaka, J. Tersoff, M. C. Reuter, and F. M. Ross, *Science* **316**, 729 (2007).
  - <sup>11</sup>B. J. Kim, J. Tersoff, S. Kodambaka, M. C. Reuter, E. A. Stach, and F. M. Ross, *Science* **322**, 1070 (2008).
  - <sup>12</sup>E. Sutter and P. Sutter, *Nano Lett.* **8**, 411 (2008).
  - <sup>13</sup>S. Hofmann, R. Sharma, C. T. Wirth, F. Cervantes-Sodi, C. Ducati, T. Kasama, R. E. Dunin-Borkowski, J. Drucker, P. Bennett, and J. Robertson, *Nat. Mater.* **7**, 372 (2008).
  - <sup>14</sup>O. G. Shpyrko, R. Streitel, V. S. K. Balagurusamy, A. Y. Grigoriev, M. Deutsch, B. M. Ocko, M. Meron, B. Lin, and P. S. Pershan, *Science* **313**, 77 (2006).
  - <sup>15</sup>O. G. Shpyrko, R. Streitel, V. S. K. Balagurusamy, A. Yu. Grigoriev, M. Deutsch, B. M. Ocko, M. Meron, B. Lin, and P. S. Pershan, *Phys. Rev. B* **76**, 245436 (2007).
  - <sup>16</sup>P. S. Pershan, S. E. Stoltz, S. Mechler, O. G. Shpyrko, A. Y. Grigoriev, V. S. K. Balagurusamy, B. H. Lin, and M. Meron, *Phys. Rev. B* **80**, 125414 (2009).
  - <sup>17</sup>S. Mechler, P. S. Pershan, E. Yahel, S. E. Stoltz, O. G. Shpyrko, B. Lin, M. Meron, and S. Sellner, *Phys. Rev. Lett.* **105**, 186101 (2010).
  - <sup>18</sup>A. L. Pinardi, S. J. Leake, R. Felici, and I. K. Robinson, *Phys. Rev. B* **79**, 045416 (2009).
  - <sup>19</sup>V. Halka, R. Streitel, and W. Freyland, *J. Phys. Condens. Matter* **20**, 355007 (2008).
  - <sup>20</sup>T. U. Schüllli, R. Daudin, G. Renaud, A. Vaysset, O. Geaymond, and A. Pasturel, *Nature (London)* **464**, 1174 (2010).
  - <sup>21</sup>A. L. Greer, *Nature (London)* **464**, 1137 (2010).
  - <sup>22</sup>P. W. Sutter and E. A. Sutter, *Nat. Mater.* **6**, 363 (2007).
  - <sup>23</sup>H. E. Fischer, G. J. Cuello, P. Palleau, D. Feltin, A. C. Barnes, Y. S. Badyal, and J. M. Simonson, *Appl. Phys. A* **74**, S160 (2002).
  - <sup>24</sup>S. F. Mughabghab, *Atlas of Neutron Resonances: Resonance Parameters and Thermal Cross Sections Z = 1–100*, 5th ed. (Elsevier, Amsterdam, 2006).
  - <sup>25</sup>S. Takeda, H. Fujii, Y. Kawakita, Y. Kato, S. Fujita, Y. Yokota, and S. Kohara, *Mater. Sci. Eng. A* **449-451**, 590 (2007), and private communication.
  - <sup>26</sup>H. Fujii, S. Tahara, Y. Kato, S. Kohara, M. Itou, Y. Kawakita, and S. Takeda, *J. Non-Cryst. Solids* **353**, 2094 (2007).
  - <sup>27</sup>S. Takeda, H. Fujii, Y. Kawakita, S. Tahara, S. Nakashima, S. Kohara, and M. Itou, *J. Alloys Compd.* **452**, 149 (2008).
  - <sup>28</sup>S.-H. Lee and G. S. Hwang, *J. Chem. Phys.* **127**, 224710 (2007).
  - <sup>29</sup>A. Pasturel, E. S. Tasci, M. H. F. Sluiter, and N. Jakse, *Phys. Rev. B* **81**, 140202(R) (2010).
  - <sup>30</sup>D. Ma, A. D. Stoica, and X.-L. Wang, *Nat. Mater.* **8**, 30 (2009).
  - <sup>31</sup>R. Evans, R. J. F. Leote de Carvalho, J. R. Henderson, and D. C. Hoyle, *J. Chem. Phys.* **100**, 591 (1994).
  - <sup>32</sup>R. J. F. Leote de Carvalho and R. Evans, *Mol. Phys.* **83**, 619 (1994).
  - <sup>33</sup>P. S. Salmon, *J. Phys. Condens. Matter* **18**, 11443 (2006).
  - <sup>34</sup>J. Baumgartl, R. P. A. Dullens, M. Dijkstra, R. Roth, and C. Bechinger, *Phys. Rev. Lett.* **98**, 198303 (2007).
  - <sup>35</sup>P. S. Salmon, R. A. Martin, P. E. Mason, and G. J. Cuello, *Nature (London)* **435**, 75 (2005).
  - <sup>36</sup>P. S. Salmon, *J. Phys. Condens. Matter* **17**, S3537 (2005).
  - <sup>37</sup>P. S. Salmon, A. C. Barnes, R. A. Martin, and G. J. Cuello, *Phys. Rev. Lett.* **96**, 235502 (2006).
  - <sup>38</sup>P. S. Salmon, A. C. Barnes, R. A. Martin, and G. J. Cuello, *J. Phys. Condens. Matter* **19**, 415110 (2007).
  - <sup>39</sup>P. S. Salmon, *J. Phys. Condens. Matter* **19**, 455208 (2007).
  - <sup>40</sup>J. M. Brader, R. Evans, and M. Schmidt, *Mol. Phys.* **101**, 3349 (2003).
  - <sup>41</sup>C. Grodon, M. Dijkstra, R. Evans, and R. Roth, *Mol. Phys.* **103**, 3009 (2005).
  - <sup>42</sup>H. E. Fischer, A. C. Barnes, and P. S. Salmon, *Rep. Prog. Phys.* **69**, 233 (2006).
  - <sup>43</sup>T. E. Faber and J. M. Ziman, *Philos. Mag.* **11**, 153 (1965).
  - <sup>44</sup>V. F. Sears, *Neutron News* **3**(3), 26 (1992).
  - <sup>45</sup>H. Bertagnolli, P. Chieux, and M. D. Zeidler, *Mol. Phys.* **32**, 759 (1976).
  - <sup>46</sup>J. F. Jal, C. Mathieu, P. Chieux, and J. Dupuy, *Philos. Mag. B* **62**, 351 (1990).
  - <sup>47</sup>R. M. Waghorne, V. G. Rivlin, and G. I. Williams, *J. Phys. F* **6**, 147 (1976).
  - <sup>48</sup>Ph. Mangin, G. Marchal, C. Mourey, and Chr. Janot, *Phys. Rev. B* **21**, 3047 (1980).
  - <sup>49</sup>J. H. Chang, *ENDFPLOT 2.0 - Cross Section Plotter* (Korea Atomic Energy Research Institute). Available at [<http://atom.kaeri.re.kr/endfplot.shtml>].
  - <sup>50</sup>P. S. Salmon, *J. Phys. F* **18**, 2345 (1988).
  - <sup>51</sup>P. S. Salmon, S. Xin, and H. E. Fischer, *Phys. Rev. B* **58**, 6115 (1998).
  - <sup>52</sup>P. S. Salmon, *Proc. R. Soc. London, Ser. A* **445**, 351 (1994).
  - <sup>53</sup>W. Hoyer and R. Jödicke, *J. Non-Cryst. Solids* **192-193**, 102 (1995).
  - <sup>54</sup>H. Kimura, M. Watanabe, K. Izumi, T. Hibiya, D. Holland-Moritz, T. Schenk, K. R. Bauchspiess, S. Schneider, I. Egry, K. Funakoshi, and M. Hanfland, *Appl. Phys. Lett.* **78**, 604 (2001).
  - <sup>55</sup>M. Watanabe, K. Higuchi, A. Mizuno, K. Nagashio, K. Kuribayashi, and Y. Katayama, *J. Cryst. Growth* **294**, 16 (2006).
  - <sup>56</sup>M. Pani, F. Merlo, and M. L. Fornasini, *Z. Kristallogr.* **214**, 108 (1999).
  - <sup>57</sup>H. Nakashima, A. Thamizhavel, T. D. Matsuda, Y. Haga, T. Takeuchi, K. Sugiyama, R. Settai, and Y. Ōnuki, *J. Alloys Compd.* **424**, 7 (2006).
  - <sup>58</sup>A. S. Sefat, A. M. Palasyuk, S. L. Bud'ko, J. D. Corbett, and P. C. Canfield, *J. Solid State Chem.* **181**, 282 (2008).
  - <sup>59</sup>A. F. Wells, *Structural Inorganic Chemistry*, 5th ed. (Clarendon, Oxford, 1984), p. 79.
  - <sup>60</sup>J. Weissmüller, *J. Non-Cryst. Solids* **142**, 70 (1992).
  - <sup>61</sup>A. Filipponi and A. Di Cicco, *Phys. Rev. B* **51**, 12322 (1995).
  - <sup>62</sup>S. Gruner, J. Marczinke, and W. Hoyer, *J. Non-Cryst. Solids* **355**, 880 (2009).

- <sup>63</sup>Y. Fujinaga, K. Kusaba, Y. Syono, H. Iwasaki, and T. Kikegawa, *J. Less-Common Met.* **170**, 277 (1991).
- <sup>64</sup>M.-C. Bellissent-Funel, P. J. Desré, R. Bellissent, and G. Tourand, *J. Phys. F* **7**, 2485 (1977).
- <sup>65</sup>P. Hopkins and M. Schmidt, *J. Phys. Condens. Matter* **22**, 325108 (2010).
- <sup>66</sup>T. Freltoft, J. K. Kjems, and S. K. Sinha, *Phys. Rev. B* **33**, 269 (1986).
- <sup>67</sup>N. W. Ashcroft and J. Lekner, *Phys. Rev.* **145**, 83 (1966).
- <sup>68</sup>C. L. Farrow, P. Juhas, J. W. Liu, D. Bryndin, E. S. Božin, J. Bloch, Th. Proffen, and S. J. L. Billinge, *J. Phys. Condens. Matter* **19**, 335219 (2007).
- <sup>69</sup>M. Scavini, M. Coduri, and M. Brunelli (private communication).
- <sup>70</sup>A. Zeidler, J. W. E. Drewitt, P. S. Salmon, A. C. Barnes, W. A. Crichton, S. Klotz, H. E. Fischer, C. J. Benmore, S. Ramos, and A. C. Hannon, *J. Phys. Condens. Matter* **21**, 474217 (2009).